Proceedings of the ASME 2015 34nd International Conference on Ocean, Offshore and Arctic Engineering
OMAE2015
May 31 - June 5, 2015, St. John's, Newfoundland, Canada

OMAE2015-42365

WAVE CARPET OPTIMIZATION VIA REAL TIME HYBRID MODELING

Thomas Börner
Department of Mechanical Engineering
University of California Berkeley
Berkeley, California 94720
Email: thomas.boerner@berkeley.edu

M.-Reza Alam
Department of Mechanical Engineering
University of California Berkeley
Berkeley, California 94720
Email: reza.alam@berkeley.edu

ABSTRACT

Real time hybrid modeling as a structured approach of implementing a real time control system has been proven as an efficient strategy to assess and optimize wave energy converter. In this paper an existing real time hybrid modeling framework for wave energy converter is reviewed, in which the main problem is divided into multiple sub-domains. Each sub-domain uses a preferred method, e.g. experimentally and/or computationally, which contributes to solve the main initial problem as a whole. An interface including actuators and sensors enables the simultaneously running sub-domains to communicate in a closed control loop in "real time". Specifically, the entire power takeoff of a novel WEC called the "Wave Carpet", which is classified as a submerged pressure differential device, is shifted into the computational domain. The interaction of the WEC's absorber unit with incident waves is left in the experiment due to its highly nonlinear characteristics. An extended setup allows to reveal further optimization potential of the novel converter design as a case study. Results of the converter behavior under variable wave states, and for different characteristics of the simulated PTO units are presented. In particular, the presented results show the expected broad band absorption capability of the Wave Carpet by closer examination of the influence of variable PTO unit resistance coefficients on the total, and also on the individual units' performance.

INTRODUCTION

Although computational simulation codes have experienced rapid improvements in terms of effectiveness and capability and numerical implemented methods, even for dynamic analysis, have steadily increased their potential, direct experimental testing is still necessary [1]. Experimental investigation is often the only way to assess complex, coupled structures, or to observe particular physical phenomena. Examples of such problems include those involving complicated turbulent and highly nonlinear flows or problems with impact forces such as sloshing and slamming due to wave breaking. Accurate simulation in such research fields are usually extremely time consuming. Especially, when the response characteristic of a dynamic system is not well understood, experimental testing is the only accurate way to assess the system's working principles, or to validate a corresponding numerical simulation [1]. On the other hand there exist particular groups of problems easy to be treated numerically, while experimental investigation is difficult or even non-practical (e.g. multi-physics processes like hurricanes). Yet, there is a third group of problems that cannot be fully modeled experimentally, nor numerically, but can be divided into multiple sub-problems. While the main aim is still to solve the initial problem as a whole, for each of the sub-domains there exist a preferred technique (numerical or experimental) to solve the particular domain. Complex systems involving more than one scaling factor, for instance, may require a matching of multiple characteristic numbers, which for some cases is simply impossible (e.g. a floating object under the combined action of wind and waves would require the unfeasible matching of both, Froude

number and Reynolds number). Receiving valid results from a direct numerical simulation, particularly in the wave domain and under strong wave conditions including relevant nonlinear effects would require very fine computational meshing. Moreover, simulation under a broad system parameter range can potentially get very time consuming.

In Hybrid Simulation, identified and separated domains may not have an own solution while being completely disjointed. In fact, the methodology of Hybrid Modeling implicates, that ultimately the main initial problem can only be solved as a whole. Thus, an appropriate communication between the sub-domains has to be maintained. This requires at least one interface, coupling the domains and facilitating an exchange of information. If the sub-problems are strongly coupled, and thus cannot be solved independently, and if at least one of the domains is of experimental nature, then the entire hybrid modeling must be performed in "real time". Hence, the communication between the domains through the interface is one of the major challenges in setting up a hybrid modeling framework. Moreover, the closer this framework can proceed to real time, the higher the resolution of small scale physical phenomena is and thus, for valid investigation very small loop times are required. However, the rapid improvements in both, computational capabilities and experimental techniques (e.g. sensor rate improvements and reduced actuator latencies) enable a close to real time communication between domains, which allows the assessment of even strongly coupled sub-domains, such as problems in fluid dynamics.

In a hybrid simulation framework, signals from sensors at the interface are interpreted as physical variables, (e.g. pressure, speed) and represent the input for the computational domain, respectively the simulation. In each loop either the kinematic quantities, e.g. displacements of the interface and/or forces exerted on the interface are calculated. Depending on the experimental domain and its physical constraints, this may require geometric transformation or condensation of degrees of freedom. The command signals are subsequently send to actuators for the corresponding action to be applied on the interface. The altered interface modifies the experimental domain, which now contains new initial conditions for the simulation. At the beginning of the next time step the continuous measurements enclose this new status of the modified experimental domain and the loop continues. To ensure a high resolution, the period for one loop has to be reduced to just a fraction of a second (the target time scale is less than 10 msec). In fact, the degree on which the hybrid modeling framework can operate close to real time determines the resolution of small scale phenomena, comparably how the fineness of numerical meshes affect simulation results. While the domain assignment and modeling is based on the principles of the hybrid modeling scheme which is a common tool in the field of seismic-resistant civil engineering [2], the actuators are controlled using a velocity driven close control scheme. Such closed control schemes were for instance used in experiments [3–5] and simulations [6] to find optimum latching strategies for WECs, but were also used in other fields of fluid dynamics such as wave propulsion [7].

A hybrid modeling framework, including a power takeoff (PTO) simulation, a domain interface, and a matching experimental domain was designed to assess the performance of a newly developed WEC design as a case study [8]. In this paper, an extended setup is presented to show further optimization potential of the device, called the "Wave Carpet". The Wave Carpet is a seabed mounted pressure-differential wave energy harvester [9–11] holding a flexible absorber mat, fully submerged and connected to the seabed by reciprocating piston pumps as PTO units. The flexible mat oscillates up and down under the load of overpassing waves, and exerts vertical forces on the pumps resulting in fluid being pumped. Yet, experimental modeling of a scaled Wave Carpet with reciprocating pumps yielded limited accuracy due to the fact that waves and pumps do not scale down similarly. The wave and absorber mat components are scaled down by Froude and Cauchy numbers, which do not interfere with each other, while pumps are scaled down by the Reynolds number that cannot be matched with Froude scaling. In fact, in a small scale lab test the flow in the pump can barely go beyond laminar, making predictions less correct [13].

In the real time hybrid framework, the fluid-structure interaction is kept in the initial experimental setup, whereas the PTO units are removed from the experiment and their response to the hydrodynamic forces is simulated. A velocity driven control scheme is used to control actuators at a customized interface coupling the two domains. These actuators apply computed loads onto the assessed wave absorber. The real time hybrid modeling framework was already used to optimize the Wave Carpet in terms of different resistance coefficient combinations of the (virtual) PTO units and their positioning underneath the absorber mat. The experimental setup and the domain interface were recently extended to hold three actuator-sensor couples, representing one virtual PTO unit each. The extended hybrid modeling framework allows to assess the Wave Carpet's behavior under varying wave states and for different PTO characteristics. In particular, the experiments and results presented in this paper aim to show the broadband absorption potential of the novel converter design.

Wave Carpet: A Broadband and Omnidirectional Wave Energy Converter

The bionic concept of the Wave Carpet is inspired by worldwide observed phenomena of strong wave attenuation through muddy seafloors. Not only in the gulf of Mexico but almost anywhere with a very muddy seafloor it is observed that mud banks and seafloor clay can extract significant amounts of energy from overpassing surface gravity waves in a strong interaction process [14, 16–18]. These observations have led to the principle idea

of the Wave Carpet, that if mud is capable of extracting a substantial share of energy out of incident waves, a synthetic compliant seabed-mounted mat acting as a mud-layer must be likewise [9–11]. If a suitable PTO is included (e.g. a spring-damper system) the device can be used as an efficient wave energy absorber. The proposed Wave Carpet can theoretically absorb the entire energy content of incident waves (narrow or broadband) hence has a theoretical efficiency of unity [1] [9, 10]. Moreover, the Wave Carpet has a broad bandwidth of high-performance. This property makes it more suited to realistic ocean environments where waves typically form a wide spectrum of different frequencies. Next to this, the concept yields further advantages, such as an omni-directional absorption capability and high survivability against storm surges, owing to the fact that the device is submerged.

In previous work, mud was investigated theoretically and computationally in the linear and weakly nonlinear regimes [9, 10]. It was found, that the linearized form of the governing equations admits two modes of motion: a surface-mode and a bottom-mode. While damping of surface-mode waves is higher for longer waves, the damping of a bottom-mode wave is higher for shorter waves. A weakly nonlinear analysis also showed that the rate of energy extraction increases for steeper incident surface waves [9]. A first proof of concept was proposed by Lehmann [11] and results of an improved experimental setup including three customized double acting reciprocating pumps as PTO units were presented [12]. These preliminary experimental results showed, that the analytic and computational studies are yet limited to several idealized assumptions. A finite length and width lead to diffraction from sides and the two ends and viscous and frictional effects obviously need to be considered. Furthermore, the finite and discrete number of PTO units and their response, particularly under reciprocating motion, which is a characteristic of the motion that ocean wave energy devices undergo, is typically very nonlinear (e.g. due to saturation). The latter mentioned effects significantly affect the performance of the Wave Carpet compared with linear and weakly nonlinear inviscid modeling. The fundamental challenge is, that on one hand numerical consideration of these effects are extremely time-consuming. On the other hand experimental investigation on a wide range and number of PTO units is cost and time expensive. Moreover, the range of usable PTO units is limited, since power takeoffs must be scaled down differently than the Wave Carpet (forced by scaling rules).

To addressed this challenge a real time hybrid modeling framework as elaborated in the introduction is used to quickly, yet very accurately study the performance of the Wave Carpet under the action of a broad range of PTO units.

[1] The 100% efficiency in the *absorption* is also expected to be achievable in practice since the natural counterpart, i.e. mud, can too completely damp energy of overpassing waves (see e.g. [14, 16–18])

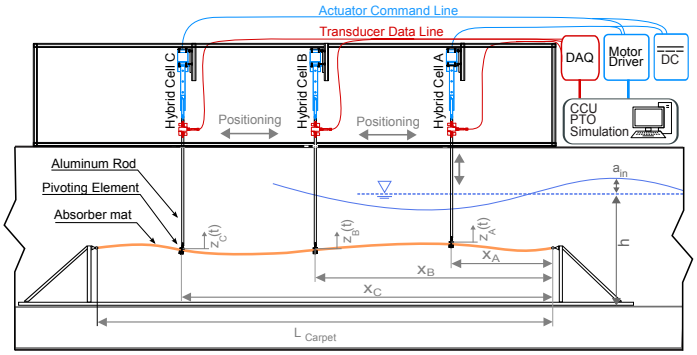

FIGURE 1: Drawing of the hybrid modeling setup including the Wave Carpet's absorber mat inside the wavetank, and the hybrid modeling structure attached to it. The domain interface was extended to hold three hybrid cells A, B and C, which are installed into a supporting structure (100 cm high and 240 cm long).

Experimental Domain Setup

The Wave Carpet's major components are identified as the "absorber mat", bundling absorbed energy of incident waves and guiding it to discrete power takeoff points, and the "PTO system" itself. The current scaled prototype uses double acting reciprocating piston type pumps as PTO units [11]. Since the wave interaction with the flexible mat can potentially be highly nonlinear, hence complex and difficult to simulate, the absorber mat is left in the initial experiment. To investigate the performance of the Wave Carpet under a broad range of PTO parameters the PTO units are simulated, and thus were removed from the initial experimental setup. Figure 1 shows the schematic of the extended hybrid modeling setup including three hybrid cells.

Next to the main physical components of the absorber device the hybrid framework comprises of three main categories: While the actuator units execute the forward feed from the PTO simulation, the sensor units are force transducers which provide the feedback from the experiment. Additionally, mechanical connections ensure the physical coupling of the absorber device and the hybrid framework components as well as the sensor and actuator units for combined operation.

Units of all three main categories are combined to assemble a "hybrid cell", replacing one PTO unit as shown in fig. 2. To operate the actuator unit, a power supply (b) and a high speed stepper driver (a) are used to control the high torque NEMA 23 stepper motor (c) with an ultra fine step resolution of 2000 $^{steps}/_{rev}$. The stepper motor is run in a velocity controlled "jog" mode, solely accelerating or decelerating between set velocities. A linear ball screw actuator (e) with a maximum stroke length of 20 cm is used to convert the rotational motion from the stepper motor into a linear stroke. The stepper driver can also be categorized as an additional sensor, tracking the position of the actuator

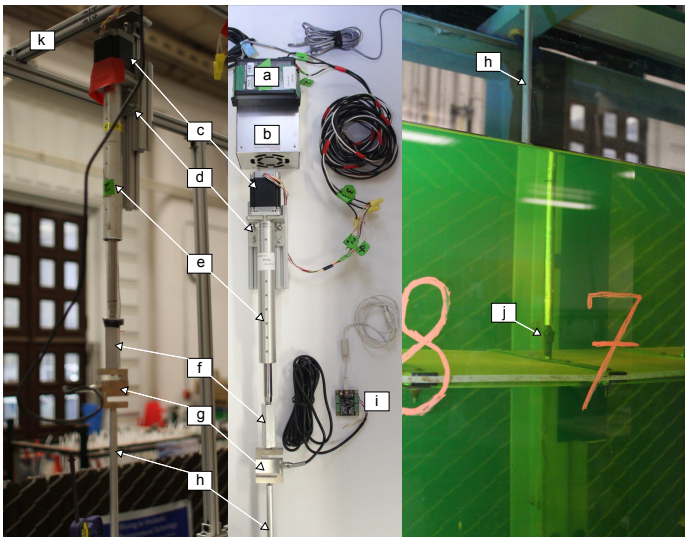

FIGURE 2: The middle picture shows the components of one hybrid cell, including the stepper motor driver (a) on top of the power supply (b). Both of these parts are wired to the stepper motor (c). The S-type loadcell (g) is installed in series through a connection element (f) to the linear actuator rod (e). A one inch diameter aluminum rod (h) couples the hybrid cell to the absorber mat using pivoting elements (j) (right picture). The force signal of the loadcell is read by a DAQ board (i). The left side shows a hybrid cell installed to the supporting frame (k) using a metal bracket (d).

rod and measuring displacements of the absorber mat. The force transducer unit requires a signal amplifier board (i), which simultaneously represents the data acquisition (DAQ) unit. The board is capable of reading four sensors simultaneously with a frequency of 125 Hz. S-type loadcells (g) provide precise force signals at a low signal to noise ratio (SNR) and furthermore yield the advantage, that only forces induced from vertical carpet displacements are measured.

A "hybrid cell" was constructed by coupling the actuator and sensor in series via a small aluminum block (f). Altogether three of these hybrid cells were built and installed to a rigid aluminum supporting frame, placed on top of the wave tank directly above the absorber mat. Each of the hybrid cells is mounted to metal brackets (d) which are screwed to separated crossbeams (k) of the supporting frame. To connect the hybrid cells to the absorber carpet, aluminum rods with small ball joint pivoting elements are used. The pivoting elements protect the actuator thread and other parts from non vertical forces.

Computational Domain

For effective implementation of the PTO simulation NI LabView 2013 was used. The code consists of six major loops: A safety loop observes the actuator rod limits, providing sensorless stall protection of the stepper motors and a motor control loop is used to manually control the actuators. Next to this, an actuator displacement request loop for position tracking, a force signal acquisition loop reading the S-type loadcells, and the power takeoff simulation loop are part of the code. Additionally, the post processing and data logging loop are included in the code. Fig. 3 provides an overview of the computational domain showing the connections and relations of the loops. One of the major challenges of the computational domain is to synchonize the different loops to ensure a correct processing of matching data packages. This challenge was addressed using synchonization commands and a global variable, which can circumvent the normal data flow by passing data from one place or loop to another without the use of the regular connection wires in Labview. Yet, the achievable overall hybrid loop time still is strongly dependent on the kind of the PTO simulation. Models which solely include a linear damper simulation can achieve loop times of $\delta t_{Hybrid,PTO} = 9ms$, while a simulation of any spring-damper combination (e.g. Kelvin-Voigt or Maxwell model) takes an increased loop time of up to $\delta t_{Hybrid,PTO} = 33ms$. This deviation can be explained by the additional displacement request, z_i, of linear actuator i. The request delay is caused by a reading limitation on the stepper driver's exit port.

To derive governing equations for the PTO simulation, on each of the discrete PTO connection points on the Wave Carpet the dynamic force equilibrium in the vertical z-direction is used as

$$\sum_j \vec{F}_{i,j}(t) = \vec{F}_{i,ext}(t) + \vec{F}_{i,damper}(t) + \vec{F}_{i,spring}(t) = 0 \quad \forall i \in N \quad (0.1)$$

Here, the term $\vec{F}_{i,ext}(t)$ combines the impinging wave and inertia forces and is equal to the forces measured by the loadcells. $\vec{F}_{i,damper}(t) = b_i\, \dot{z}_i(t)$ and $\vec{F}_{i,spring}(t) = c_i\, z_i$ represent the counter forces for a Voigt model including a viscose damper and a linear spring. The use of the Kelvin-Voigt model is partly to best present how the hybrid modeling setup works, and partly motivated by the recent findings that a Wave Carpet with a Kelvin-Voigt actuation model can give high efficiencies [9]. A velocity driven control scheme of the actuator is used, making it necessary to solve equation 0.1 for $\dot{z}_i$:

$$\dot{z}_i = -\frac{F_{ext,i} + c_i\, z_i}{b_i} \qquad \forall i \in N \qquad (0.2)$$

In the experiment the Wave Carpet already includes the needed springiness of the Voigt model. Elastic fiberglass beams, attached in longitudinal direction to be bottom side of the absorber mat were selected by an estimation of the needed elasticity and with the aim to not consider any extra linear springs

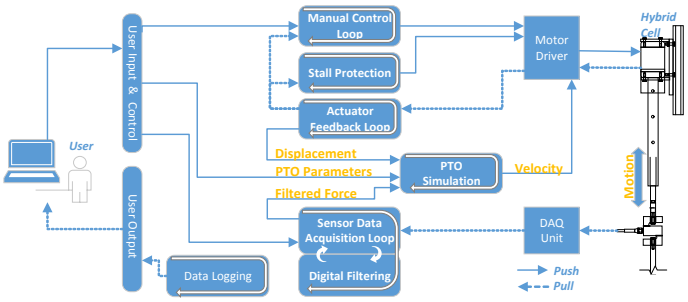

FIGURE 3: Overview of the computational domain including six major loops and their connections. For the sake of clarity no connections to the data logging loop are shown. Velocity commands are send to the linear actuator by the PTO simulation loop which receives necessary input data from the actuator feedback loop, the DAQ loop and the PTO model parameters from the user.

in the PTO simulation. This design furthermore provides a continuous springiness along the longitudinal axis of the absorber mat, rather than discrete spring elements on the PTO connection points. Thus, the characteristic spring stiffness of the virtual PTO units in equation (0.2) is set to $c_i = 0$. Due to the strong coupling of the simulation input signal, respectively the force, and the output motion of a hybrid cell, filtering was identified to be highly necessary. The filter design challenge in the here presented application is the real-time aspect, demanding a low latency low-pass filter with minimal group delay and a narrow transition band. Skogstad et al. [20] proposed a method for designing digital IIR filter with special focus on minimal group delays, resulting in the implementation of a customized first order elliptical IIR filter.

Verification tests were conducted separately for each of the constructed hybrid cells, to validate that a realistic model of the power takeoff has been implemented. By placing masses of known weights on a tableau mounted onto an upwards pointing hybrid cell the constant gravitation of the mass acts on the cell. As the used Voigt model does not include any simulated spring the actuator rod drives inwards, just as a contracting damper would. As the actuator rod reaches the very low limit of the stroke the mass was removed. The induced energy and average power can thus be manually calculated and compared to the one computed from the virtual model. These validation tests yielded only a very small error of just a couple of percent, with a tendency to lower errors by the use of higher resistance coefficients b_i. The mean power output error for a damping coefficient range of $b_i \in [400-4000]\frac{Ns}{m}$ is in the range of $3.5\%-1\%$. Next to this, internal loop periods were measured using code internal stopwatches. These tests showed, that even the largest loop periods of the PTO simulation do not exceed a loop time of 9 ms. Moreover, to examine the latency between feeding the motor with a velocity command and the actual movement of the motor, the high sensitivity of the attached loadcell was used. The difference between the time when the command was sent to the stepper driver and the peak response of the attached loadcell was recorded by the datalogging function. A constant time lag of 8 ms was found. As the sampling rate of the loadcell is limited to a minimum of 8 ms the intrinsic timelag between sending a command and its execution must be equal or less than these 8 ms.

Results and Discussion

All experiments presented in this paper were conducted in O'Brien wave tank (L x W x D=30 x 0.45 x 2.4 meter) of the University of California, Berkeley. A paddle-type wave-maker is capable of generating monochromatic waves with a frequency up to 0.9 Hz, which run over an artificial beach to a reduced water depth. The Wave Carpet with a length of $L_{Carpet} = 2.73m$ is installed at a distance of 10.7m from the wave-make at a water depth of $h = 0.75m$ on the beach. On one of the transparent side planes of the wave tank, 2 meters upstream from the Wave Carpet, an optical wave height measurement system is installed. By using the method described by Goda and Suzuki [21] wave parameters can be measured precisely. Wave reflection on the far end of the wave tank was measured for an empty tank and was found to be very low due to the use of effective wave baffles. Two types of experiments, one under a fixed wave state and one for variable wave states, were conducted with different experimental setups as the following overview states:

Experiment	PTO units	Wave State	Resistance Coefficient b_i
PTO Resistance Coefficient	2	$f = 0.23$Hz $H = 0.07$m	$b_i \in [400, 5000]$
Variable Wave State	3	$f \in [0.11, 0.63]$Hz $H \in [0.02, 0.16]$m	$b_i = [1000, 2000, 3000, 4000]$

To assess how the characteristic resistance properties of the PTO units affect the efficiency of the WEC and how the individual units contribute to the overall efficiency of the device, two hybrid cells were equally distributed over the longitudinal axis of the absorber mat resulting in $[x_A, x_B] = [1/3\, L_{Carpet}, 2/3\, L_{Carpet}]$ (c.f. fig. 1). 990 different combinations of the resistance coefficients b_A and b_B were tested in the range of $b_A, b_B \in [400, 5000]\frac{Ns}{m}$. For each test, the total power of the Wave Carpet and the individual power of each of the simulated PTO units was measured over a time period of Δt=40 seconds. Longer periods do not significantly change the average power output any more. Thus, good estimations of the average power outputs $\overline{P_i} = E_i/\Delta t$ are obtained. For the resistance coefficient combination tests the wave frequency, $f = 0.23Hz$, and waveheight, $H = 0.07m$, were kept constant to avoid further complexity in interpretation of results. The dispersion relation leads to a wavenumber of k=0.54 m^{-1}, and wavelength of λ=11.63m at the given water depth for this wave state. To quantify the Wave Carpet's performance in absorbing energy the ratio of the virtual generated power $\overline{P_i}$ is divided by the wave energy flux $P_{wave} = 1/2\rho g a^2 C_g W$. Here,

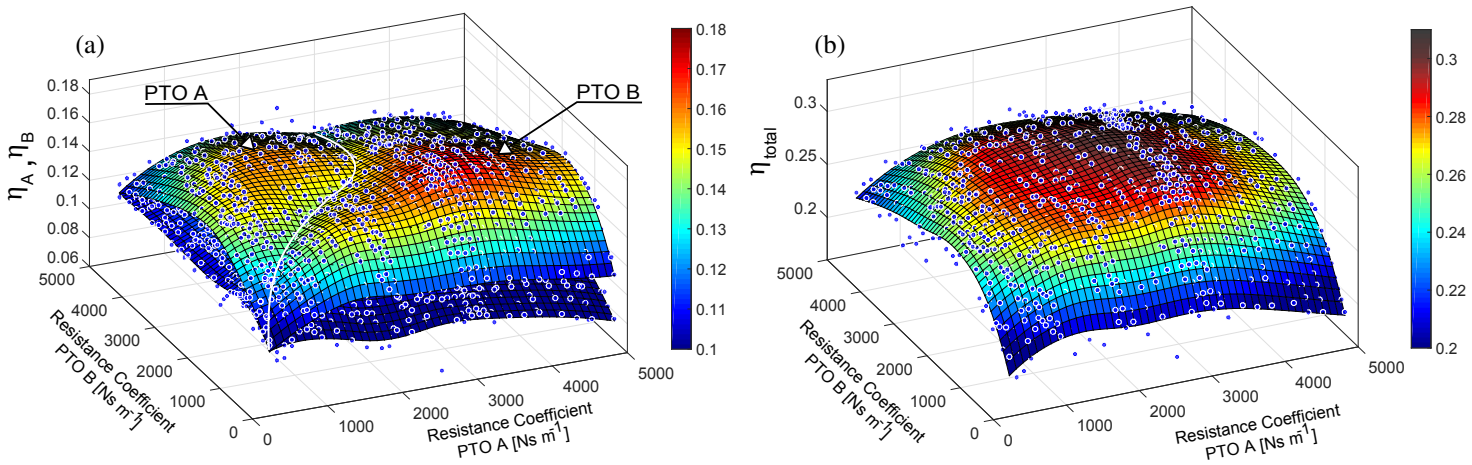

FIGURE 4: Individual efficiencies η_A, η_B (a) of the virtual PTO units and total efficiency η_{total} (b) of the Wave Carpet plotted for 990 damping combinations of two hybrid PTO cells. The incident wave parameters were kept constant for all measurement points. Resistance combinations with either one of the coefficients below $1000\frac{Ns}{m}$ yield a low total efficiency, while the maximum total efficiency of $\eta_{total} = 31.92\%$ is found in the area of a combination of $[b_A, b_B] \sim [3000, 2900]\frac{Ns}{m}$. The white line in (a) indicates the points of equal efficiency for PTO unit A and B.

W=0.45m is the wave tank width and C_g the group velocity of the incident waves. The individual and overall efficiency when using N PTO units can thus be written as

$$\eta_{total} = \sum_{1}^{N} \eta_i = \sum_{1}^{N} \frac{\overline{P_i}}{P_{wave}} \quad \forall i \in N \tag{0.3}$$

Fig. 4 (a) shows the individual efficiency of each of the PTO units A and B, whereas the surface in fig. 4 (b) represents the overall efficiency. Clearly, the efficiencies in both plots are functions of the PTO units' resistance coefficients b_A and b_B. Least square surfaces are fitted to the actual measured data points which are shown in the graphs as blue dots. While the maximum total efficiency of $\eta_{total} = 32\%$ was measured using a combination of $b_A, b_B \sim 3000, 2900\frac{Ns}{m}$, the individual efficiency peak of PTO B is found for a combination of $b_B, b_B \sim 3400, 2000\frac{Ns}{m}$ with $\eta_B = 17.4\%$, respectively for unit A at $b_A, b_B \sim 1700, 3200\frac{Ns}{m}$ with $\eta_A = 16.4\%$. Additionally in fig. 4 (a) the intersection line of both surfaces is highlighted in white color. This iso-efficiency line is not always at the points where $b_A = b_B$. In fact, for relative high resistance coefficients ($b_A, b_B > 2500\ \frac{Ns}{m}$) the major part of energy is absorbed by PTO unit B, mounted further downstream onto the absorber mat. Apparently, for large resistance coefficients unit A shows an overdamped behavior. This results in a change of the incident wave height due to the reduced water level while running over the first part of the absorber mat (note, that the carpet has a finite height). The altered wave then applies a higher load further downstream on PTO unit B, which is now able to absorb a larger amount of energy out of the wave. Hence, for a given wave spectra and matching resistance coefficients of the PTO units a broad band of waves with different wave height may be harvestable due to the influence of the Wave Carpet on the overpassing waves itself. Moreover, this explains the bulge shaped surface of the overall efficiency in 4 (b), showing a comparatively moderate gradient for a broad range around the global peak. Despite of the fact that the PTO units are able to operate independently they are still coupled through the absorber mat and thus have a positive and in some cases negative influence on each other (edges of the surfaces in fig. 4).

A common characteristic of wave energy absorber designs is the strong dependence of the performance on their location of deployment in the ocean. To assess the Wave Carpet's total efficiency as a function of the PTO characteristic for variable wave states the extended setup with three hybrid cells was used. The units were again equally distributed over the carpet length ($[x_A,\ x_B,\ x_C] = [1,\ 5,\ 9]$). Four sets of experiments were conducted. For each set uniform characteristic resistance coefficients of the virtual PTO units ($b_A = b_B = b_C =$ 1000, 2000, 3000, 4000 $\frac{Ns}{m}$) were used. Figure 5 shows the contour plots of the total efficiency as a function of the monochromatic wave periods ranging from $T \in [1.58,\ 9.1]\ s$ and variable wave heights $H \in [0.02,\ 0.16]\ m$. The axis limits of the plots are defined by these wave parameter ranges. Related wave frequencies are in the range of $f \in [0.63,\ 0.11]\ Hz$ and lie within the excitation frequency of the wave-maker. Each set includes more than 60 measurements to which quadratic spline surfaces were fitted. For wavestates which are out of the limits of the plots, efficiencies of $\eta = 0$ are assumed, yielding an estimation to the

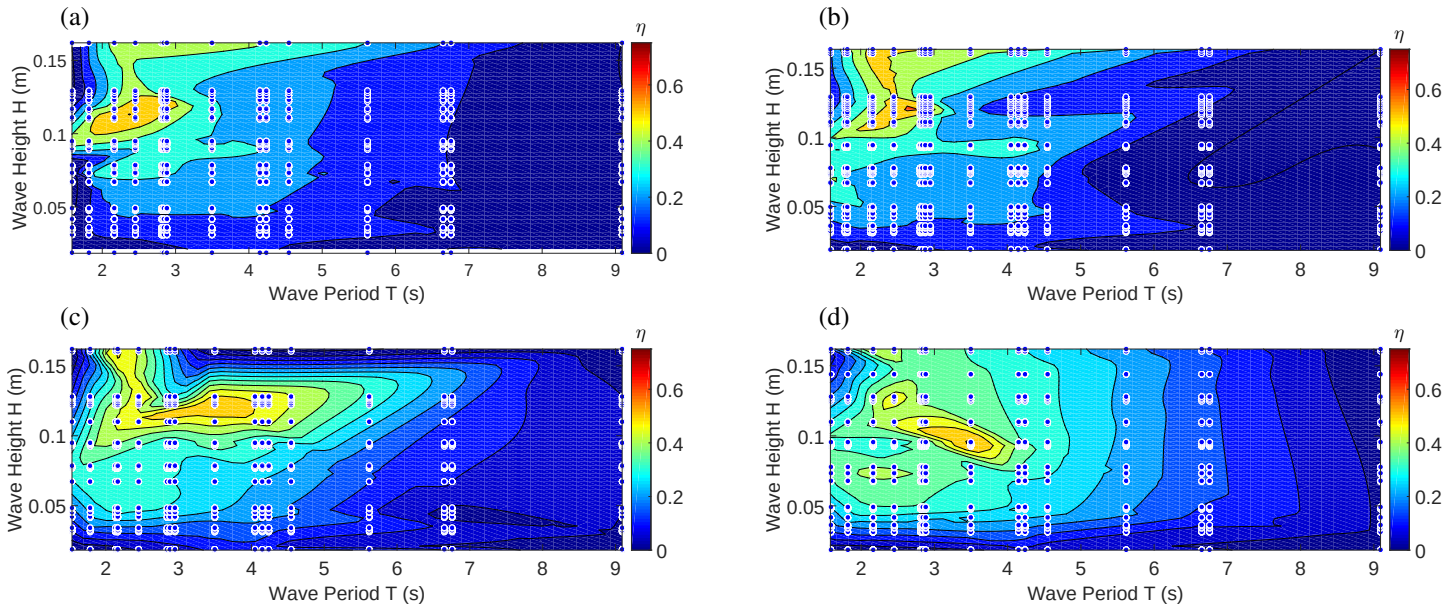

FIGURE 5: Total device efficiency using three (virtual) PTO units. a) - d) show the efficiency for four uniform damping cases ($b_A = b_B = b_C = 1000,\ 2000,\ 3000,\ 4000\ \frac{Ns}{m}$) as a function of the incident wave period T and waveheight H. For all cases the PTO units were equally distributed over the carpet length. A clear shift and enlargement of the efficient area can be observed for larger values of b_i.

safe side. For all resistance coefficient cases (a), (b), (c) and (d) high efficiencies in the range of $50-60\%$ can be found. Yet, the efficiency peaks occur for different wave states. The highest total efficiency of $\eta = 60.6\%$ is found for resistance coefficients of $b_i = \ 2000\ \frac{Ns}{m}$ at $T = 2.82\ s$ and $H = 0.12\ m$. Respectively, for case (a), (c) and (d) peak efficiencies of 57.0%, 54.1% and 56.3% were measured. Note, that while this efficiency seems high, it is not unexpected as Wave Carpet is known to be capable of providing a theoretical efficiency of unity in ideal cases [9]. A shift of the maximum efficiency areas from low periods for cases with low damping (a) to higher periods for higher damping cases ((c), (d)) can be observed. This can be explained by an (over)damped absorber mat, which cannot follow the quickly changing pressure differential of low period waves any more. Furthermore a comparison of the plots (a) to (d) shows, that with a rise in the resistance coefficients a much larger range of incident waves in terms of the wave period (horizontal enlargement), as well as in terms of the waveheight (vertical enlargement) can efficiently be absorbed. Especially, the results for high resistance coefficients ((c), (d)) confirm the above described self regulating mechanism of the Wave Carpet (cf. fig. 4). Such kind of experiments can furthermore be used to design a customized power takeoff for a given deployment side. For many potential field sides the wave spectra and frequency distribution (H_sT_p distributions) are precisely known. By comparing such H_sT_p distributions with the scaled laboratory tests optimal PTO parameter for a specific side can be found.

Concluding Remarks

The real time hybrid simulation approach can be used to investigate problems that cannot be fully simulated, nor entirely experimentally assessed. For instance problems involving complex small scale phenomena or those who require to simultaneously satisfy numerous scaling rules are either time consuming to simulate and sometimes even impossible to realize experimentally. Real time hybrid simulation allows the separation of such problems into multiple sub-domains which can be solved with a suitable method being either more practical, cost effective, or even more accurate. Yet, especially for strongly coupled problems, these sub-domains cannot be solved independently from each other and thus a close coupling through an interface is necessary. In case of wave energy converter, for instance, incident waves affect the performance of PTO units. In return, the power takeoff's response can significantly affect the wave field near the wave energy absorber. Considering these effects in numerical simulations requires significant computational effort [22] [23], but becomes immanent by the use of real time hybrid modeling. Specifically, during the optimization stage and in cases where a large number of system parameters are to be testes, simulating the PTO of a WEC and using close control schemes offers a fast and efficient testing alternative. The method can significantly reduce the cost of actual PTO implementations, particularly in the prototype stage, and furthermore circumvent limitations in scalability of PTO systems. Thus, hybrid modeling can be seen as a cost and time efficient alternative in the performance assessment

and optimization of WECs.

In this paper an extended setup of the real time hybrid modeling framework was presented to reveal further optimization potential of the Wave Carpet. Results of a more detailed assessment of the influence of PTO configurations on the individual efficiency of the PTO units are presented and explanatory approaches of the Wave Carpet's working principle are given. Moreover, it is shown how the hybrid simulation technique allows optimization of the Wave Carpet in matching variable operating sides, which is one of the major challenges in the field of ocean wave energy conversion. Optimized PTO unit parameters were found to achieve the predicted [9] broadband wave absorption potential of the Wave Carpet.

Acknowledgements

We would like to thank Professor Khalid Mosalam, Dr. Mostafa Shakeri, Marcus Lehman, Ryan Elandt and Ricardo Maldonado. Funding for this research is provided by U.C. Berkeley's Committee on Reseach, and American Bureau of Shipping.

REFERENCES

[1] J. E. Carrion, B. F. Spencer Jr., Model-based strategies for real-time hybrid testing, NSEL, University of Illinois at Urbana-Champaign, 2007.

[2] F. J. Jiang Wang, Jin-Ting Wang, Real-time dynamic hybrid testing for soilstructure interaction analysis, Soil Dynamics and Earthquake Engineering Vol. 31.

[3] J. Hals, J. Falnes,T. Moan, Constrained Optimal Control of a Heaving Buoy Wave Energy Converter, CeSOS, Norwegian University of Science and Technology (NTNU), 2009.

[4] R. Henderson, Design, simulation, and testing of a novel hydraulic power take-off system for the Pelamis wave energy converter, Renewable Energy Vol.31, pp. 271-283, 2006.

[5] A. Babarit, A. H. Clément, Optimal latching control of a wave energy device in regular and irregular waves, Applied Ocean Research Vol. 28, Elsevier, pp. 77-91, 2006.

[6] J. Hals, J. Falnes, T. Moan, Constrained Optimal Control of a Heaving Buoy Wave Energy Converter, CeSOS, J. Offshore Mech. Arct. Eng., Vol. 133, 2010.

[7] E. Bockmann, S. Steen, Experiments with actively pitch-controlled and spring-loaded oscillating foils, Applied Ocean Research Vol. 48, Elsevier, pp. 227-235, 2014.

[8] T. Börner, M.-R. Alam, Real time hybrid modeling for ocean wave energy converters, Renewable & Sustainable Energy Reviews, Vol. 43, pp. 784-795, 2015.

[9] M.-R. Alam, Nonlinear analysis of an actuated seafloor-mounted carpet for a high-performance wave energy extraction, Proceedings of the Royal Society A: Mathematical, Physical and Engineering Sciences. doi 10.1098/rspa.2012.0193doi:10.1098/rspa.2012.0193.

[10] M.-R. Alam, A flexible Seafloor Carpet for High-Performance Wave Energy Extraction, in: Proceedings of the ASME 2012 31st International Conference on Ocean, Offshore and Arctic Engineering OMAE2012, 2012, Brazil (OMAE2012-84034), 2012. doi:10.1098/rspa.2012.0193.

[11] M. Lehmann, R. Elandt, H. Pham, R. Ghorbani, M. Shakeri, M.-R. Alam, An artificial seabed carpet for multidirectional and broadband wave energy extraction: Theory and Experiment, in: Proceedings of 10th European Wave and Tidal Energy Conference, EWTEC2013, Aalborg, Denmark, 2013.

[12] M. Lehmann, R. Elandt, M. Shakeri, M.-R. Alam, The Wave Carpet: Development of a Submerged Pressure Differential Wave Energy Converter, Proceedings of 30th Symposium on Naval Hydrodynamics, Hobart, 2014.

[13] G. Vetter, E. Thiel, U. Stork, Reciprocating Pump Valve Design, in: Proc. 6lh lnt. Pump Users Symp., Houston TX USA, pp. 39–52, 1989.

[14] H. G. Gade, Effects of a non-rigid, impermeable bottom on plane surface waves in shallow water, Journal of Marine Research, Vol. 16, pp. 61–82, 1958.

[15] S. Elgar, B. Raubenheimer, Wave dissipation by muddy seafloors, Geophysical Research Letters 35 (7), pp. 1–5, 2008. doi:10.1029/2008GL033245.

[16] R. Silvester, Coastal Engineering, Vol. 1, Elsevier, 1974.

[17] H. Macpherson, P. G. Kurup, Wave damping at the Kerala mudbanks, southwest India, Indian Journal of Marine Science, Vol. 10, 1981.

[18] A. Sheremet, G. W. W. Stone, Observations of nearshore wave dissipation over muddy sea beds, Journal of Geophysical Research 108, pp. 1–11, 2003. doi:10.1029/2003JC001885.

[19] B. Carlson, Communication Systems: an Introduction to Signals and Noise in Electrical Communication, McGraw-Hill, New York, 1968.

[20] A. Skogstad, S. Holm, M. Hovin, Designing digital IIR low-pass differentiators with multi-objective optimization, 11th International Conference on Signal Processing (ICSP), Vol. 1, 2012.

[21] Y. Goda, Y. Suzuki, Estimation of incident and reflected waves in random wave experiments, Proc. of 15th coastal engng conference, Honolulu, Hawaii, pp. 828–845, 1976.

[22] E. Agamloh, A. Wallace, A. von Jouanne, Application of FluidStructure Interaction Simulation of an Ocean Wave Energy Extraction Device, American Institute of Aeronautics and Astronautics 25th Wind Energy Symposium, 2006.

[23] A. Muetze, J. Vining, Ocean Wave Energy Conversion - A survey, Industry Applications Conference 41st IAS Annual Meeting, Vol.3, 2006.